Paleoceanography and Paleoclimatology

RESEARCH ARTICLE
10.1029/2018PA003465

Centennial-Scale SE Pacific Sea Surface Temperature Variability Over the Past 2,300 Years

James A. Collins[1], Frank Lamy[1], Jérôme Kaiser[2], Nicoletta Ruggieri[1], Susann Henkel[3], Ricardo De Pol-Holz[4,5], René Garreaud[5,6], and Helge W. Arz[2]

[1]Alfred Wegener Institute Helmholtz Centre for Polar and Marine Research, Am Alten Hafen 26, Bremerhaven, Germany, [2]IOW - Institute for Baltic Sea Research, Warnemünde, Germany, [3]Alfred Wegener Institute Helmholtz Centre for Polar and Marine Research, Am Handelshafen 12, Bremerhaven, Germany, [4]GAIA-Antártica, Universidad de Magallanes, Punta Arenas, Chile, [5]Center for Climate and Resilience Research (CR)[2], University of Chile, Santiago, Chile, [6]Department of Geophysics, University of Chile, Santiago, Chile

Key Points:
- Chilean margin sea surface temperature displays cooling from 1,100 to 600 cal yr BP pointing to a reduction in Southern Ocean deep convection
- Multicentennial sea surface temperature variability is out of phase with Northern Hemisphere temperatures
- This suggests roles for internal Southern Ocean Centennial Variability and/or phasing of individual ENSO-SAM events

Correspondence to:
J. A. Collins,
jcollins@gfz-potsdam.de

Citation:
Collins, J. A., Lamy, F., Kaiser, J., Ruggieri, N., Henkel, S., De Pol-Holz, R., et al. (2019). Centennial-scale SE Pacific sea surface temperature variability over the past 2,300 years. *Paleoceanography and Paleoclimatology*, *34*, 336–352. https://doi.org/10.1029/2018PA003465

Received 21 AUG 2018
Accepted 14 FEB 2019
Accepted article online 16 FEB 2019
Published online 14 MAR 2019

Abstract Detailed temperature reconstructions over the past 2,000 years are important for contextualizing modern climate change. The midlatitude SE Pacific is a key region in this regard in terms of understanding the climatic linkages between the tropics and southern high latitudes. Multicentennial timescale temperature variability remains, however, poorly understood, due to a lack of long, high-temporal-resolution temperature records from this region and from the southern high latitudes in general. We present a unique alkenone sea surface temperature (SST) record from 44°S on the southern Chilean margin in the SE Pacific spanning the last 2,300 years at decadal resolution. The record displays relatively large changes including a cooling transition from 14 to 12.5 °C between 1,100 and 600 cal yr BP, in line with other Chile margin SST records and coeval with Antarctic cooling. This cooling is attributable to reduced Southern Ocean deep convection, driven by a late Holocene sea-ice increase in the Weddell Sea associated with increased El-Niño Southern Oscillation variability. Superimposed on the late Holocene cooling, we observe multicentennial timescale SST variability, including relatively cool SSTs (12.5 °C) from 950 to 500 cal yr BP, corresponding to the Medieval Climate Anomaly, and warmer SSTs (13 °C) from 500 to 200 cal yr BP, corresponding to the Little Ice Age. These oscillations may reflect either multicentennial internal variability of the Southern Ocean deep convection and/or multicentennial variability in the phasing of El-Niño Southern Oscillation and Southern Annular Mode events.

1. Introduction

Instrumental records indicate that although global temperatures are on the rise, the SE Pacific (Falvey & Garreaud, 2009; Vuille et al., 2015) and the Pacific sectors of the Southern Ocean (Armour et al., 2016) have cooled over the last few decades. This is in stark contrast to the West Antarctic Peninsula (G. J. Marshall et al., 2006) and rest of West Antarctic Ice Sheet (Steig et al., 2009), which have shown a marked warming. The Southern Ocean cooling is thought to be related to upwelling of cool waters in the Southern Ocean (Armour et al., 2016), while the Peninsula warming is thought to be related to a shift toward the positive phase of the Southern Annular Mode (SAM; Thompson et al., 2011; Thompson & Solomon, 2002). However, these instrumental records only extend back to the 1950s (and satellite data only to the 1980s) making it difficult to unravel which patterns and mechanisms are typical on multicentennial timescales. The southern Chile margin (Figure 1a) represents an interesting study region in this sense because it lies under the influence of the SAM, a mid-latitude to high-latitude phenomenon, and also the El-Niño Southern Oscillation (ENSO), a tropical phenomenon. Both phenomena cause major changes in atmospheric and ocean circulation (Figures 1b and 1c; see section 2.2) and are thought to have undergone marked variability over the last 2,000 yr (Moreno et al., 2014; Villalba et al., 2012; Yan et al., 2011), perhaps related to Total Solar Irradiance (Yan et al., 2011). In addition to these two major influences, it is thought that the Southern Ocean exhibits internal centennial variability (Southern Ocean Centennial Variability; SOCV), which involves buildup of heat at middepth that is periodically released to the surface during periods of vertical mixing, resulting in surface temperature changes in the Southern Ocean and Chilean margin (Latif et al., 2013; Martin et al., 2013; Park & Latif, 2008; Zhang, Delworth, & Jia, 2017). However, determining which influences were most important remains challenging because the multicentennial-scale temperature evolution of the Southern Hemisphere midlatitudes

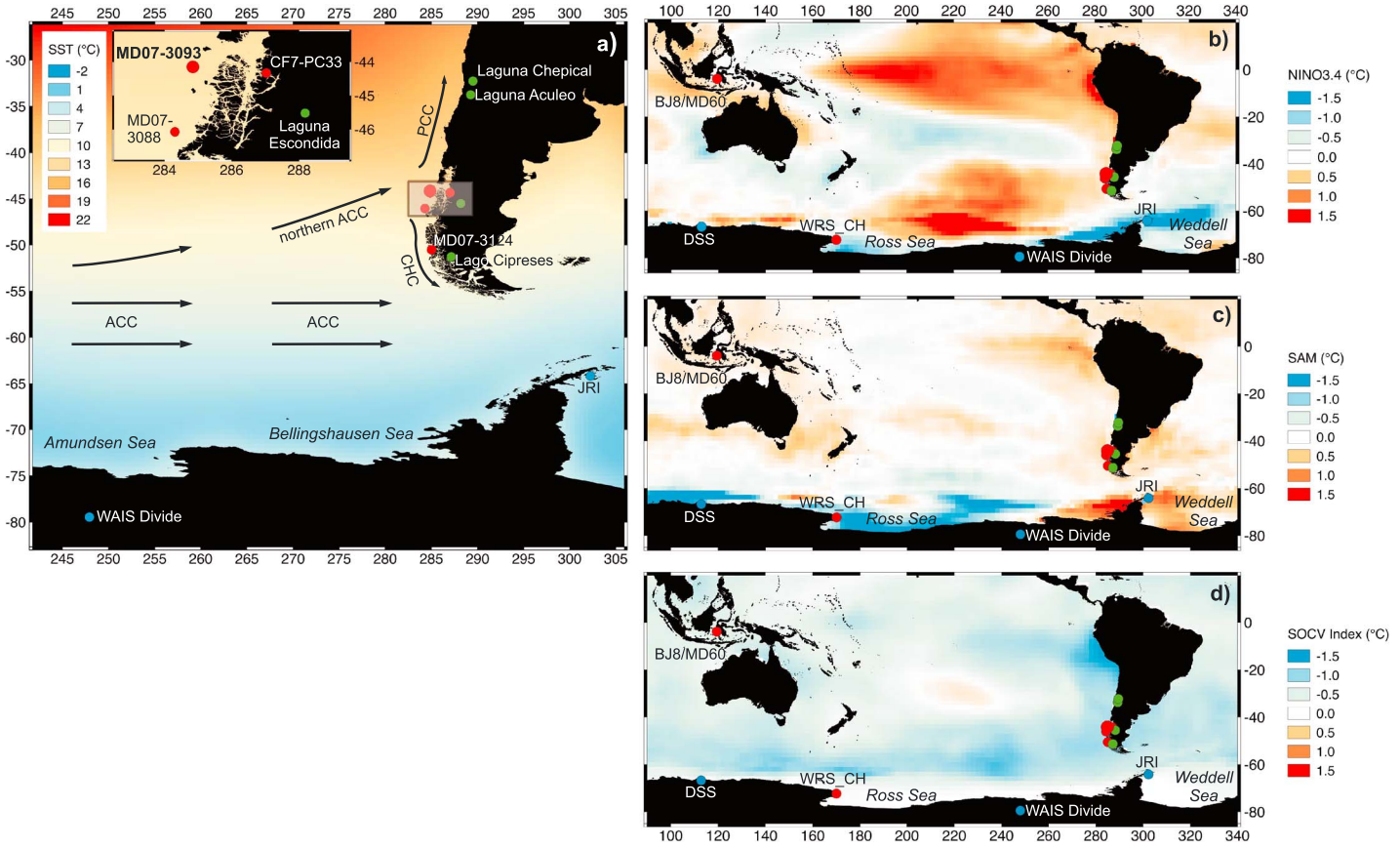

Figure 1. Maps of modern SST and anomalies due to El-Niño Southern Oscillation (ENSO), Southern Annular Mode (SAM), and Southern Ocean Centennial Variability (SOCV). (a) Modern-day SE Pacific SSTs. Colors indicate mean annual SST (Locarnini et al., 2013). Sites include MD07-3093 (this study) and others mentioned in the main text. GeoB7186-3 is at the same site as MD07-3093. Antarctic Circumpolar Current (ACC), Cape Horn Current (CHC), and Peru Chile Current (PCC) are marked. (b) ENSO SST composite anomaly (January–December) based on El-Niño years minus La-Niña years defined using NINO3.4 SST using the NCEP/NCAR Reanalysis (Kalnay et al., 1996). (c) SAM SST composite anomaly (January–December) based on positive SAM years minus negative SAM years defined using the National Oceanic and Atmospheric Administration (NOAA) SAM index (Gong & Wang, 1999; Kalnay et al., 1996). (d) Composite map of the SOCV index (°C) showing the cool minus the warm index (Latif et al., 2013), based on the ERSSTv5 data set over the period 1854–2017 (Huang et al., 2017). After detrending the record, cool (warm) index years are defined as those with an index lower (higher) than 1.2 std dev below (above) the mean (Latif et al., 2013). WAIS = West Antarctic Ice Sheet; JRI = James Ross Island; SST = sea surface temperature.

is still relatively poorly constrained, mainly due to a lack of archives that are both long and high-resolution.

Previous work on reconstructing past decadal-centennial temperature variability from the midlatitude SE Pacific region is largely based on a range of tree-ring and lake sediment records from southern South America (Neukom et al., 2011; Neukom & Gergis, 2012). Although annually resolved, South American tree rings mostly only extend back over a few centuries (Neukom & Gergis, 2012, and references therein), albeit with some exceptions (Lara & Villalba, 1993), and their interpretation may be complicated by sensitivity to precipitation (Boninsegna et al., 2009, and references therein). Lake sediments have provided high-resolution (annual-decadal) and longer records (Boës & Fagel, 2008; de Jong et al., 2013; Elbert et al., 2015, 2013; von Gunten et al., 2009). Although these temperature records display a similar evolution over the last three centuries, differences in temperature evolution between the sites have been noted further back in time (de Jong et al., 2013), perhaps highlighting a high degree of spatial heterogeneity of temperature on these timescales, as is also seen over the last few decades (Villalba et al., 2003). Many of these records have been included in compilation reconstructions for South America (Neukom et al., 2011; PAGES-2K-Network, 2013), and the result suggests relatively warm conditions around the time of the Medieval Climate Anomaly (MCA; 1,000 to 700 cal yr BP) and cool conditions around the time of the Little Ice Age (LIA; 550 to 100 cal yr BP), albeit at slightly different timing with the Northern Hemisphere (Neukom et al., 2014). However, it

should be noted that in southern South America, only the 1,150-yr long lake sediment record from Laguna Aculeo (33°50′S; 70°54′W; 355 m above sea level) in central Chile (von Gunten et al., 2009) extends beyond 570 cal yr BP in these compilations. Moreover, past reconstructions of the SAM index (Abram et al., 2014), which are based on temperature, also rely on this reconstruction from 34°S beyond 570 cal yr BP; although at this latitude, SAM exerts a relatively minor effect on temperature over the period of the instrumental record (Garreaud et al., 2009; Gillett et al., 2006). Overall, this highlights that improved temporal and spatial coverage of temperature reconstruction is needed for the SE Pacific-southern South America region.

As well as South American records, Antarctic ice cores provide long and high-resolution temperature records from the high latitudes of the SE Pacific region. The James Ross Island (JRI) ice core located on the Antarctic Peninsula (Figure 1a) suggests warming over the last 600 years (Mulvaney et al., 2012), interpreted as reflecting a trend toward more positive SAM (Abram et al., 2014). Compilations of several ice core records throughout East and West Antarctica (PAGES-2K-Network, 2013) show a general cooling over the last 1,000 yr, which would be in line with a shift toward positive SAM (Abram et al., 2014). The cooling is most pronounced in the West Antarctic Ice Sheet (WAIS) Divide ice core but is not uniform throughout East and West Antarctica: It is less pronounced at DSS (Law Dome) and Plateau Remote and not evident at EPICA Dronning Maud Land, reflecting the complexity of Antarctic climate variability (PAGES-2K-Network, 2013).

Further inferences about past oceanic and atmospheric circulation patterns can be made from sea surface temperature (SST) reconstructions from the Southern Ocean and SE Pacific. Existing alkenone SST reconstructions from the southern Chilean margin tend to cover a longer timespan than the South American lake and tree records, albeit at lower temporal resolution (25 yr or less). The Chilean margin SST records generally show a late Holocene cooling transition between about 1,300 and 600 cal yr BP, although the timing varies between records (Caniupán et al., 2014; Kaiser et al., 2005; Lamy et al., 2002; Mohtadi et al., 2007; Neukom et al., 2014; Sepúlveda et al., 2009). Further south, a TEX_{86} SST record from ODP1098, located to the west of the West Antarctic Peninsula, displays warm conditions between 1,700 to 350 cal yr BP, attributed to La-Niña-like conditions (Shevenell et al., 2011). Nonetheless, the lower temporal resolution of these records allows only limited inferences to be made regarding multicentennial-scale SST changes over the last 2,000 yr, and thus the evolution of SE Pacific SSTs during the MCA (1,000–700 cal yr BP) and LIA (550–100 cal yr BP) is not well constrained.

In this study we focus on understanding the SST evolution of the SE Pacific on multicentennial timescales. We estimate SST using the alkenone unsaturation index measured on sediments from a new marine core MD07-3093 located at 44°S on the Chile margin. The high sedimentation rates on the southern Chile margin provide a unique sediment archive that is both long (2,300 yr) and of high-resolution (5-yr sampling resolution). Such archives are otherwise rare in the ocean-dominated midlatitude to high latitudes of the Southern Hemisphere.

2. Setting

2.1. Modern Oceanographic Setting

Surface waters are transported around Antarctica by the Antarctic Circumpolar Current (ACC; Figure 1a). This is mainly driven by the Southern Hemisphere Westerlies (SHW) as well as buoyancy forcing. The SHW exhibit maximum intensity at around 55°S (J. Marshall & Speer, 2012). The zonal wind stress of the SHW generates Ekman upwelling poleward of the SHW maximum and downwelling equatorward of the maximum. Together with the northward flowing cross-ACC surface water and poleward flowing cross-ACC deep water, this forms the Deacon Cell between 40°S and 60°S. (J. Marshall & Speer, 2012). The upwelling brings relatively warm deep water masses back to the surface and is thus an important component of the Atlantic Meridional Overturning Circulation (AMOC; J. Marshall & Speer, 2012). Surface waters are cooled and downwelled south of 60°S, forming the Antarctic Bottom Water (AABW) cell. Major sites of AABW formation are the Weddell and Ross Seas (Talley, 1999). Reduced upwelling and hence reduced AABW formation are thought to lead to surface cooling in the Southern Ocean (Zhang, Delworth, & Jia, 2017; Zhang, Delworth, & Zeng, 2017).

The surface waters reaching the MD07-3093 core site are advected northeastward by the northern branch of the ACC (often referred to as the West Wind Drift) from the central Pacific sector of the subantarctic

Southern Ocean (ca. 50–55°S) toward the Chile margin (Figure 1a; Chaigneau & Pizarro, 2005). The MD07-3093 core site, positioned at ~44°S, is at a similar latitude to the northern ACC bifurcation (Chaigneau & Pizarro, 2005). To the south of the bifurcation, the Cape Horn Current carries surface water southward toward the Drake Passage. To the north of the bifurcation, surface water is transported northward by the Peru Chile Current. Coastal upwelling occurs on the Chile margin north of about 39°S at present: South of this upwelling is much weaker due to the onshore flow of the SHW (Strub et al., 1998). However, exceptions can occur, such as during 2016, when more intense southerly winds promoted upwelling in the coastal region of western Patagonia (Garreaud, 2018).

2.2. Effect of ENSO and SAM on Chilean Margin SST

Modern-day instrumental data show that SST and surface air temperature in the SE Pacific region are affected by ENSO (e.g., Ciasto & Thompson, 2008; Yuan, 2004). El-Niño (La-Niña) events exhibit warmer (cooler) conditions in the tropical Pacific, and in summer, the warming (cooling) progressively extends in a narrow band along the South American coast toward Central and southern Chile (Figure 1b), driven by coastally trapped internal waves. In the atmosphere, ENSO is teleconnected to the southern Pacific region: El-Niño (La-Niña) generates shallowing (deepening) of the Amundsen Sea Low, causing cooler (warmer) SST and expanded (reduced) sea ice in the Bellingshausen Sea, around the West Antarctic Peninsula and in the Weddell Sea; and causing warming (cooling) and reduced (expanded) sea ice in the Ross and Amundsen Sea sectors of the Southern Ocean (Ciasto & Thompson, 2008; Garreaud et al., 2009; Yuan, 2004; Figure 1b). Along the southern Chile margin, however, ENSO SST anomalies are relatively small (Figure 1b): The largest anomalies (0.5 °C) occur in summer but are not significant during winter.

The SAM is the leading mode of climate variability in the Southern Hemisphere midlatitude to high latitudes and describes near zonally symmetric north-south movements of the midlatitude jet, observed on weekly-monthly timescales (Thompson & Wallace, 2000). The positive phase of the SAM is associated with a poleward displacement of the jet, and thus a strengthening of the eastward flow at around 60°S, weakening of the eastward flow around 40°S, and reduced surface air pressure over Antarctica (Ciasto & Thompson, 2008; Hall & Visbeck, 2002; Thompson & Wallace, 2000). The positive (negative) phase of SAM is also associated with a deepening (shallowing) of the Amundsen Sea Low, producing similar high latitude anomalies to La-Niña (El-Niño), that is, warm (cool) anomalies in the Bellingshausen and Weddell Seas and around the West Antarctic Peninsula and cool (warm) anomalies in the Ross and Amundsen Seas (Figure 1c; Fogt & Wovrosh, 2015; Holland & Kwok, 2012; Parkinson & Cavalieri, 2012; Stammerjohn et al., 2008; Steig et al., 2009; Thompson et al., 2011; Thompson & Solomon, 2002). Positive (negative) SAM results in warm (cool) SST anomalies along the southern Chilean margin. However, the anomalies are small in magnitude (Figure 1c), and the largest occur in winter. The SHW strengthening at 60°S results in colder conditions over the rest of West Antarctica and East Antarctica, as well as anomalous northward Ekman transport of cool SSTs from the Southern Ocean (Ciasto & Thompson, 2008; Hall & Visbeck, 2002; Zhang, Delworth, & Zeng, 2017).

Instrumental records covering the last 35 years show that a positive (negative) SAM state often co-occurs with La-Niña (El-Niño; Figures 2a and 2b) as previously described (Ding et al., 2012; Fogt & Bromwich, 2006; Fogt et al., 2011; Hendon et al., 2014; L'Heureux & Thompson, 2006). Thus, Niño3.4 and SAM indices exhibit a weak negative correlation that is larger in austral summer ($r \approx -0.13$). In a typical La-Niña-positive SAM coupling situation, La-Niña causes cooling on the southern Chilean margin, yet positive SAM causes warming, leading to a small net effect on Chilean margin SSTs (Figure 2c). Large SST anomalies off Chile are, however, evident when positive SAM combines with El-Niño or negative SAM combines with La-Niña. During 2000, cool conditions associated with La-Niña were followed by a sharp shift to negative SAM resulting in a major drop in SST off Chile (Figure 2c; blue bar in Figure 2). During 2009, there was a transition from La-Niña to El-Niño, but the effect was offset by the concurrent transition from a positive to negative SAM polarity, resulting in a shift to cold conditions off southern Chile (blue bar in Figure 2). During 2010, although SAM changed from negative to positive polarity (reaching +1.2 by the end of 2010), the simultaneous development of La-Niña maintained the cold SST off Chile (Figure 2c). Over the last 30 years, we also witnessed periods in which strong El-Niño events (1998 and 2016, red bars in Figure 2) developed in concert with the positive phase of SAM. For instance, a major El-Niño event began in 2015 and culminated in the austral summer of 2016 with Niño3.4 exceeding 2.5 °C. At the same time, the SAM

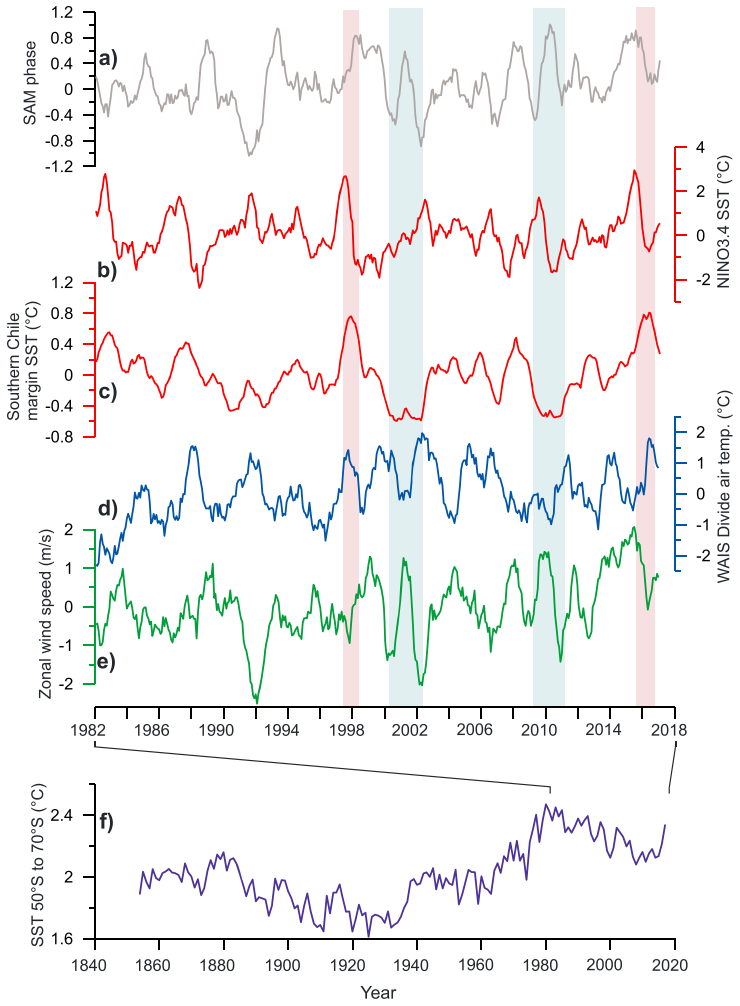

Figure 2. Instrumental time series. (a) SAM phase based on the NOAA index (Gong & Wang, 1999; Kalnay et al., 1996). (b) NIÑO3.4 SST anomaly (Kalnay et al., 1996). (c) Southern Chilean margin SST anomaly (mean for the region 41–51°S and 275–285°W). Cross correlation with SAM displays $r = 0.23$ with no lag. Cross correlation with NIÑO3.4 displays $r = 0.33$ with a lag of about 8 months. Blue bars mark southern Chilean margin cold SST anomalies and red bars warm anomalies. (d) Air temperature anomaly for the region of the WAIS Divide ice core (mean for the region 75–85°S and 245–250°W). Cross correlation with SAM displays $r = -0.20$. (e) Zonal wind strength anomaly in the southern Pacific (mean for the region 55 to 70°S and 200–280°W). Cross correlation with WAIS Divide air temperature displays $r = -0.19$. Cross correlation with SAM phase displays $r = 0.71$. (f) Zonal mean SST between 50°S and 70°S over the period 1854–2017 based on the ERSSTv5 data set (Huang et al., 2017). WAIS = West Antarctic Ice Sheet; SST = sea surface temperature; SAM = Southern Annular Mode.

index reached one of the highest positive values on record. In this case, both the positive SAM and the strong El-Niño fostered a major warming in the coastal ocean off southern Chile leading to major environmental disruptions in that region (Garreaud, 2018).

2.3. SOCV

A detailed assessment on longer timescales is difficult due to the sparseness of long instrumental data sets. Nonetheless, the Extended Reconstructed Sea Surface Temperature (ERSST) v5 data set (Huang et al., 2017) is considered suitable for the assessment of longer-term basin wide changes. This data set has been used to describe centennial temperature variability in the Southern Ocean and used to derive the Southern Ocean Centennial Variability (SOCV) index (Latif et al., 2013), which is based on zonal mean SST 50°S to 70°S over the last 160 yr (ERSSTv5: 1854 to 2017). This SST data set highlights an oscillation from warm conditions at the end of the nineteenth century to cool conditions at the start of the twentieth Century and back to warmer conditions toward the end of the twentieth Century (Figure 2f). The SST composite map (Figure 1d)

Table 1
Uncalibrated Radiocarbon Ages (Not Reservoir Corrected) for MD07-3093

Lab code	Depth (cm)	Depth (turbidite corrected; cm)	AMS ^{14}C age (yr)	Error (yr)
UCIAMS133203	68	52	630	20
UCIAMS133204	119	103	685	20
UCIAMS133205	219	197	810	20
UCIAMS133206	319	297	1,140	20
UCIAMS133207	419	391	1,420	25
UCIAMS133208	519	477	1,675	20
UCIAMS133209	669	624	2,015	20
UCIAMS133210	719	674	2,150	20
UCIAMS133211	819	773	2,420	20
UCIAMS133212	919	870	2,640	20

illustrates that centennial-scale cool SSTs on the Chile margin are in phase with the cool SSTs in the Southern Ocean over this period.

The mechanism to explain SOCV is related to the deep convection, similar to the proposed cause of Weddell Sea ice melting in the 1970s (Gordon, 1978): Gradual surface buildup of freshwater from advection or melting of sea ice acts as a cap, stalling deep convection; subsequent gradual accumulation of heat at intermediate depths eventually destabilizes the water column, generating deep convection and warming at the surface (Martin et al., 2013; Zhang, Delworth, & Jia, 2017).

3. Material and Methods

3.1. Core Material

Piston core MD07-3093 was taken in 2007 during the PACHIDERME Cruise (Kissel & Leau, 2007) at 44°09.03′S, 075°09.05′W and 1,129-m water depth (Figure 1a). This core site is located at a sediment drift site on the continental slope (Kissel & Leau, 2007). Small centimeter-scale turbidites in the core were identified with XRF scanner Fe/Ca and radiograph (sediment density) data measured every millimeter using an ITRAX core scanner, with a Cr tube operated at 30 kv and 30 mA and an exposure time of 15 s, at the Institute for Baltic Sea Research, Warnemünde. The intervals corresponding to turbidites were removed from the composite depth of the core to produce an event-free depth scale.

3.2. Age Model

The age-depth model for marine sediment core MD07-3093 is based on 10 radiocarbon measurements (Table 1) and, to assist with estimation of the surface ocean reservoir age, 17 ^{210}Pb measurements (Figures 3a and 3b). Radiocarbon was measured on 2.3–5.9 mg of *Globigerina bulloides* foraminifera at the Keck carbon cycle Accelerator Mass Spectrometry facility, University of California, Irvine. ^{210}Pb, ^{226}Ra, and ^{137}Cs were measured at the Alfred Wegener Institute, Bremerhaven. About 7 g of pulverized dry sediment were analyzed for at least 48 hr each by nondestructive gamma spectrometry using a Canberra Broad Energy GE-Detector. Unsupported ^{210}Pb (airborne, not produced in the sediment by decay of ^{226}Ra) was calculated for each sample by subtracting the supported ^{210}Pb that is based on ^{226}Ra ($^{210}Pb_{supp}$) from the measured total activity of ^{210}Pb in the sample (Figure 3a).

Previous estimates of the surface ocean reservoir age from the Chile margin tend to be higher than the global mean of 400 yr (i.e., ΔR tends to be >0). A ΔR estimate of 390 ± 160 yr was made using foram and charcoal ages of tephra from core MD07-3088 on the Chilean margin (46°04.30′S; 075°41.23′W; 1,536-m water depth) for the time period between 1,700 and 4,000 cal yr BP (Siani et al., 2013). A ΔR estimate of 380 ± 120 yr was made on co-occuring carbonate and wood in core JPC-42 from Canal

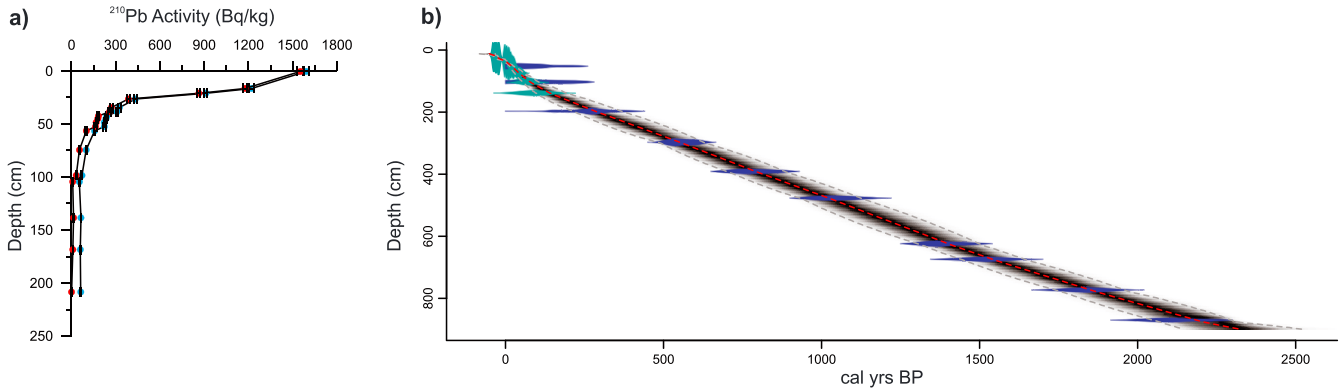

Figure 3. Age model for core MD07-3093. (a) Unsupported ^{210}Pb (red) and total ^{210}Pb (blue) versus depth profile for core MD07-3093. Error bars for the measurements are shown. Supported ^{210}Pb yielded a mean value of 49 ± 7 Bq/kg. The ^{137}Cs bomb spike was not detected, as expected in the Southern Hemisphere. (b) Age-depth model for core MD07-3093 (cal yr BP) based on ^{210}Pb (green) and radiocarbon (blue) ages.

Wide in the Chilean Fjords (49°55′S; 074°23′W; 904-m water depth) at an age of 794 cal yr BP (Caniupán et al., 2014). However, a number of other studies from further afield on the Chilean margin suggest smaller ΔR estimates, including an estimate of 165 ± 107 yr made on coastal shells at 30–33°S in central Chile (Carré et al., 2016) and 203 ± 41 yr on molluscs from the Puerto Natales region at 51°S (Ingram & Southon, 1996).

The ^{210}Pb profile displays an exponential decrease in unsupported ^{210}Pb activity with depth (Figure 3a). A turbidite was evident in the ^{210}Pb profile between 46- and 31-cm sediment depth, and depths have subsequently been corrected to account for this. The top 15 cm of sediment were absent in core MD07-3093 and CASQ core MD07-3094 (retrieved from the same site as MD07-3093), likely representing loss of the unconsolidated sediment-water interface during coring at this high sedimentation rate site. Thus, to estimate the initial ^{210}Pb content for core MD07-3093, we analyzed the uppermost 1 cm of sediment from multicore GeoB7186-1 (44°09.52′S; 075°09.52′W; 1,171-m water depth; in close proximity to MD07-3093). This exhibits ^{210}Pb activity of 1,592 Bq/kg (Figure 3a).

Ages were generated from the MD07-3093 ^{210}Pb profile using the constant rate of supply model (Appleby, 2001), which the most suitable for variable sedimentation rates. Dry bulk density was estimated based on multisensor core logger data (Kissel & Leau, 2007).

To estimate the reservoir age for MD07-3093, we input both the ^{210}Pb and radiocarbon ages into a P_Sequence routine in OxCal 4.2 (Bronk Ramsey, 2008), using the Marine13 calibration curve. This yielded a posterior ΔR of 184 ± 51 yr, in agreement with recent results of pre-bomb ΔR values for the same area (Merino-Campos et al., 2018). Due to the lack of constraints further down core, we held the reservoir age constant throughout the last 2,000 yr. To generate the age model, we used BACON2.2, using a ΔR of 184 ± 51 yr (Figure 3b). We used the following priors: accumulation shape and mean of 0.8 and 5, respectively, memory strength and mean of 30 and 0.4, respectively, section thickness of 6 cm, and ages follow a normal distribution. The BACON-derived age model provided us with Markov chain Monte Carlo estimates of combined age and proxy uncertainty. Mean confidence range (95%) on the age model is 180 yr over the last 2,300 yr and ranges between 10 yr at the top and 380 yr at the bottom (Figure 3b). The average sedimentation rate for core MD07-3093 over the last 2,300 yr is 4 m/Kyr.

3.3. Alkenone Analysis

Five hundred 1-cm-thick sediment samples were taken between 0- and 10-m depth every 2 cm using a spatula, resulting in an average sampling resolution of 5 years. Two to five grams (dry weight) of freeze dried and ground sediment was extracted using a DIONEX ASE350 accelerated solvent extractor at 100 °C using dichloromethane (DCM) for 5 min. The ketone fraction was obtained by elution of the dried lipid extract over a silica gel column (1 g, mesh size 60). To avoid coelution with the alkenones, alkyl alkenoates and the apolar fraction were first removed by elution with 5-ml Hexane/DCM 1:1, and the ketone fraction was subsequently eluted with 5-ml DCM.

Alkenone analysis was performed on an Agilent 7890A gas chromatograph equipped with a GerstelC506 Cooled Injection System (injected at 60 °C, heated at 12 °C/s, and then held at 320 °C for 5 min) and a flame ionization detector. The column was an Agilent DB-1MS column (60 m × 0.32 mm) with film thickness 0.25 μm, and helium was used as carrier gas at 1.5 ml/min. The gas chromatograph was held at 60 °C for 3 min, heated at 20 °C/min to 150 °C, heated at 6 °C/min to 320 °C, and held at 320 °C for 40 min. Duplicate analyses (n = 205) yield an analytical precision of 0.1 °C (1σ). Repeated analysis of an external alkenone standard cultured at 6 °C yielded a precision of 0.3 °C. We calculated the modified alkenone unsaturation index $U^{K'}_{37} = (C_{37:2}) / (C_{37:3} + C_{37:2})$ (Brassell et al., 1986; Prahl et al., 1988) and calculated SST using the culture calibration $U^{K'}_{37} = 0.034 \times T + 0.039$ (Prahl et al., 1988). This is confirmed by SE Pacific (Prahl et al., 2006) and global (Müller et al., 1998) core-top calibrations, the later of which has a standard error of 1.5 °C.

3.4. Statistical Methods

The timing of the main cooling transition was determined using Significant Zero crossings of derivatives (SiZer) analysis (Chaudhuri & Marron, 1999). This creates a family of Gaussian smooths for the data and for each smooth identifies the time periods during which the derivative is significantly different from

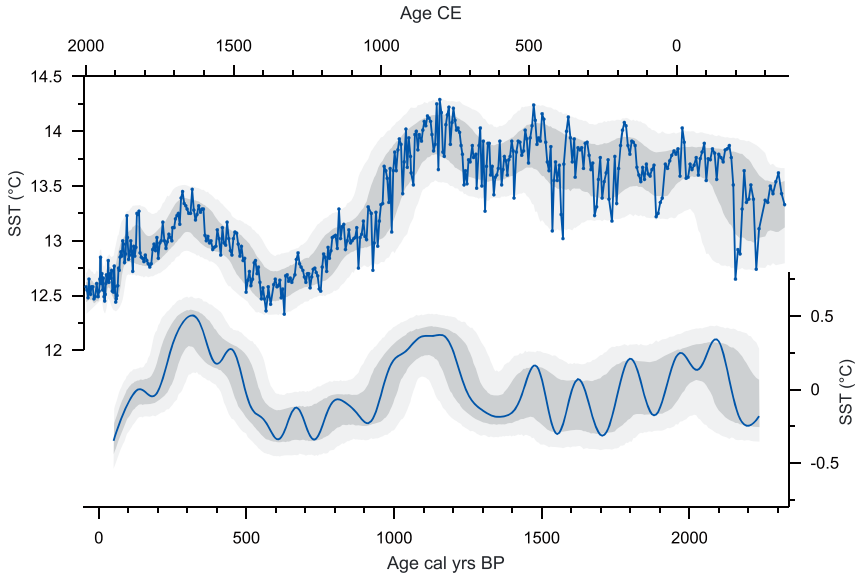

Figure 4. MD07-3093 SST record. (a) MD07-3093 alkenone SST record on the southern Chilean margin. (b) Bandpass-filtered SST showing only variability with periods between 1,000 and 100 yr. Gray confidence intervals (68% and 95%) include analytical precision and age model error. SST = sea surface temperature.

zero. The degree of smoothing is based on the Ruppert-Sheather-Wand bandwidth, the optimal smoothing for the data set (Ruppert et al., 1995).

Given existing evidence for climate variability on multicentennial timescales in the tropical Pacific (Oppo et al., 2009; Yan et al., 2011) and in southern South America (Moreno et al., 2014), we filtered our record to isolate climate variability at multicentennial timescales from that at millennial timescales. We used the Analyseries 2.0 software (Paillard et al., 1996) to bandpass filter our record with a piecewise linear filter. We filtered out millennial timescale variability (period > 1,000 yr) as well as high frequency variability (period < 100 yr).

4. Results

The core-top SST value from MD07-3093 is 12.5 °C (Figure 4a), within the alkenone-SST calibration error of the modern-day mean annual SST (12.1 °C) at the core site (Locarnini et al., 2013). The slight overestimation may be due to a small bias of the alkenone SST toward the spring and summer blooming season (Caniupán et al., 2014).

Over the past 2,300 yr, SST values range between 14.3 and 12.2 °C (Figure 4a), and hence most of the record is warmer than today. The earlier half of the record is relatively warm and stable and displays a gradual warming from 13.2 °C at 2,300 cal yr BP to 14 °C at 1,200 cal yr BP. The largest feature of the record is the cooling transition from 14 to 12.5 °C between 1,100 and 600 cal yr BP (Figure 4a). This is followed by warming to 13.5 °C at 300 cal yr BP and then cooling to 12.5 °C at present day.

Multicentennial variability is more clearly highlighted in the filtered record (Figure 4b**)** and is most pronounced over the last 1,200 year. The record exhibits relatively warm conditions during the periods 1,200–950 and 500–200 cal yr BP and relatively cool conditions during the periods 950–500 cal yr BP and 200 cal yr BP to present (Figure 4b). The mean difference between the periods is of magnitude 0.5 °C.

5. Discussion

5.1. Late Holocene Cooling

MD07-3093 SSTs display a large magnitude cooling transition of 1.5 °C between about 1,100 and 600 cal yr BP (Figure 5a). A similar magnitude cooling transition is observed in other Chilean margin SST records, including marine core GeoB7186-3 (44°08.96′S; 075°09.49′W; 1,169-m water depth; Figure 5b; Mohtadi

et al., 2007), fjord core CF7-PC33 from Jacaf fjord (44°20.00′S; 072°58.15′W; 510-m water depth; Figure 5c; Sepúlveda et al., 2009), marine core MD07-3088 (46°04.30′S; 075°41.23′W; 1,536-m water depth; Figure 5d; Haddam et al., 2018), and fjord core MD07-3124 from Canal Concepcion (50°30.96′S; 74°58.33′W; 564-m water depth; Figure 5e; Caniupán et al., 2014).

There are, however, some differences in the timing and duration of the cooling transition between the Chilean margin records. Cooling is more gradual in core GeoB7186-3 (1,550–550 cal yr BP; Figure 5b), which is from close proximity to the MD07-3093 coring site. The timing difference is probably attributable to the age model uncertainty (95%) of the two cores (± 90 yr at 1,100–600 yr BP for MD07-3093 and ± 120 yr at 1,550–550 yr BP for GeoB7186-3) and to a stronger effect of bioturbation on the lower sedimentation rate GeoB7186-3 core. Furthermore, due to its low sedimentation rate, SiZer selects a higher bandwidth (more smooth) smoothing curve for the GeoB7186-3 record.

From the same latitude as MD07-3093, fjord core CF7-PC33 from Jacaf fjord (Figure 5c) displays a similar magnitude and trend but the change is more abrupt (cooling between 1,050 to 900 cal yr BP) and SSTs in this record are slightly lower and much more variable (Caniupán et al., 2014) than our marine record. This may reflect the marked spatial and temporal salinity variations in the fjords (Schneider et al., 2014), which may modify the alkenone unsaturation index independently of temperature (Schulz et al., 2000).

The cooling was later and more gradual in cores located further south along the Chilean margin: MD07-3088, an open ocean core, displays cooling between 1,000 and 400 (Figure 5d), and MD07-3124 in Canal Concepcion displays cooling between 1,100 and 300 cal yr BP (Figure 5e). In these cases, as well as the age model uncertainty, the spatial variability of the marine reservoir age was likely an additional contributor to the uncertainty. Timing issues aside, a late Holocene cooling of about 1.5 °C is a clear feature of Chile margin SSTs.

We suggest that the SST cooling between 1,100 and 600 cal yr BP is associated with a deep circulation slowdown that was triggered by a sea ice increase, in turn related to ENSO. A shift toward stronger ENSO variability is observed at about 1,100 cal yr BP in the Lake Pallcacocha record (Figure 5f) from Ecuador (Moy et al., 2002). El-Niño events are known to increase sea ice in the Weddell Sea (Yuan, 2004). We suggest that melting of this sea ice produced a freshwater cap that was able to reduce the upwelling of the AABW, cooling the Southern Ocean and southern Chile margin SST, as has been shown in models (Park & Latif, 2008; Zhang, Delworth, & Jia, 2017). We propose that prior to 1,100 cal yr BP, AABW convection was stronger and/or more frequent, while after 600 cal yr BP, AABW convection was weaker and/or less frequent.

Southern Ocean cooling is expected to have further enhanced sea ice cover in the Southern Ocean (Park & Latif, 2008; Zhang, Delworth, & Jia, 2017). This is in accordance with two records displaying increased sea ice in the western Ross Sea at a similar timing (between 1,250 and 650 cal yr BP) to the cooling (Figure 5g; Mezgec et al., 2017). Late Holocene sea-ice increases are also observed to the west of the Ross Sea (Denis et al., 2010), to the west of the West Antarctic Peninsula (Etourneau et al., 2013), and in the Eastern Ross Sea (Mayewski et al., 2013). Associated ice-albedo and ice-insulation feedbacks (Renssen et al., 2005; Varma et al., 2012) may have contributed to the rapidity of the cooling and sea-ice expansion.

Cooling is observed in the compilation of Antarctic ice core records (PAGES-2K-Network, 2013) between 1,050 and 650 cal yr BP (Figure 5h), a similar timing to our SST record. This cooling is likely partly explained by the Southern Ocean cooling and increased sea ice cover. In addition, however, Southern Ocean cooling likely generated a poleward shift of the SHW (Latif et al., 2013; Zhang, Delworth, & Jia, 2017), further cooling Antarctica (Gillett et al., 2006). Antarctic cooling is most pronounced in the WAIS Divide ice core (Figure 5i), which shows evidence for cooling between 1,150 and 900 cal yr BP (Fegyveresi et al., 2011; WAIS-Divide-Project-Members, 2013). Modern instrumental records show that temperature at WAIS Divide is weakly negatively correlated ($r = -0.19$) to the strength of the zonal winds in the Amundsen-Bellingshausen Sea sector of the southern Pacific (Figures 2d and 2e). Stronger, more zonal winds coincide with weaker meridional winds in this region (weaker warm, northerly flow) and hence cooler temperatures at WAIS Divide. Thus, the Antarctic cooling (Figures 5h and 5i) may represent a shift from more meridional, northerly flow prior to 1,100 cal yr BP toward more zonal flow subsequent to 600 cal yr BP. This mechanism would not, however, explain why JRI does not display temperature transition at this time (Figure 5j). One possible explanation for this might be a concurrent shift in the position of the Amundsen Sea Low, which is also important for temperatures in West Antarctica (Hosking et al., 2013).

10.1029/2018PA003465

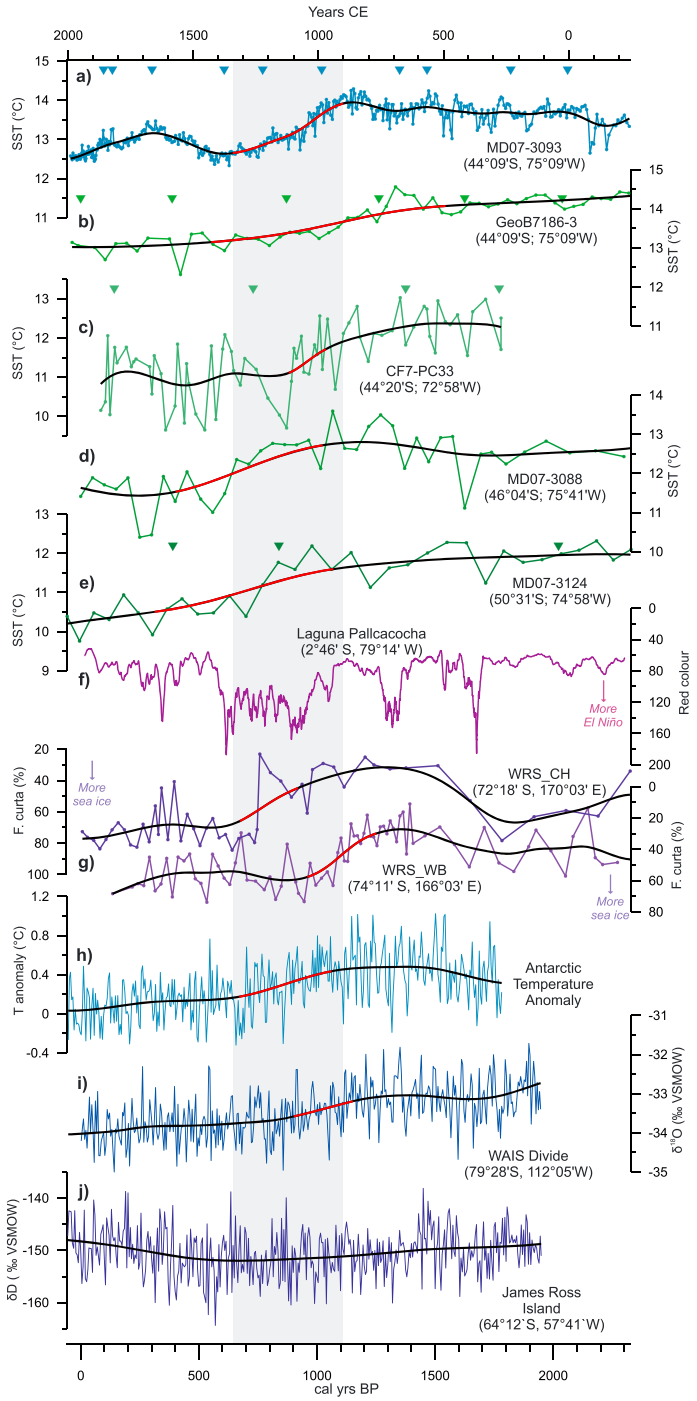

Figure 5. Late Holocene cooling on the southern Chilean margin and in Antarctica. (a) Alkenone SST record from MD07-3093 (this study). (b) Alkenone SST from GeoB7186-3 (Mohtadi et al., 2007). Similar to MD07-3093, the age model was calculated with BACON2.2, using the Marine13 calibration and $\Delta R = 184 \pm 51$ yr. (c) Alkenone SST from CF7-PC33 in Jacaf fjord (Sepúlveda et al., 2009). Ages were recalibrated with IntCal13 and calculated using BACON2.2. (d) Alkenone SST record from core MD07-3088 (Haddam et al., 2018). (e) Alkenone SST record from MD07-3124 in Canal Concepcion fjord 51°S (Caniupán et al., 2014). Ages were recalibrated with IntCal13 and calculated using BACON2.2 with a reservoir age of 780 yr. (f) El-Niño Southern Oscillation variability from Laguna Pallcacocha (Moy et al., 2002). (g) Sea ice reconstructions from cores WRS_CH and WRS_WB, in the western Ross Sea (Mezgec et al., 2017). (h) PAGES 2K Antarctic temperature anomaly (PAGES-2K-Network, 2013). (i) $\delta^{18}O$ from the WAIS Divide ice core (WAIS-Divide-Project-Members, 2013). (j) δD from the James Ross Island ice core (Mulvaney et al., 2012). Thick lines represent the Ruppert-Sheather-Wand smooth. Periods of significant cooling are highlighted as a thick red line. All annual ice core data were first binned into 5-year bins (shown in h–j; a temporal resolution similar to MD07-3093), before SiZer analysis. Gray bar marks the timing of cooling in the MD07-3093 record. Diamonds are radiocarbon age control points from the SST records. SST = sea surface temperature; WAIS = West Antarctic Ice Sheet.

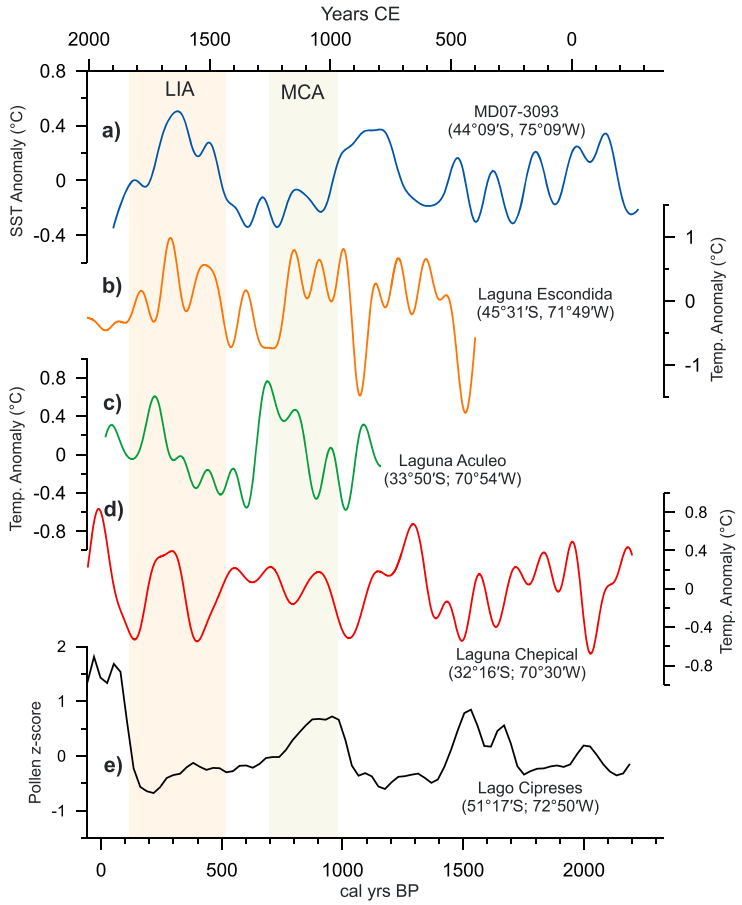

Figure 6. Comparison with South American terrestrial temperature records. (a) Southern Chilean margin SST from MD07-3093. (b) Annual temperature anomaly from Laguna Escondida (Elbert et al., 2013). (c) Summer (December–February) temperature anomaly from Laguna Aculeo (von Gunten et al., 2009). (d) Summer (November–February) temperature anomaly from Laguna Chepical (de Jong et al., 2013). (e) Pollen z-score values from Lago Cipreses, 52°S in southwestern Patagonia: Higher/lower values indicate warmer/cooler conditions and positive/negative Southern Annular Mode (Moreno et al., 2014). All are bandpass filtered so as to show variability with periods between 1,000 and 100 yr. SST = sea surface temperature; LIA = Little Ice Age; MCA = Medieval Climate Anomaly.

Most South American terrestrial temperature records do not feature a cooling transition between 1,100 and 600 cal yr BP (Figure 6; described in section 5.2). The absence of a cooling transition may be attributable to the poleward shift of the SHW. Increased westerly and northerly flow into southern South America during summer causes terrestrial warming (Moreno et al., 2014; Thompson et al., 2011) and thus could have counteracted any influence of SST cooling.

5.2. Multicentennial-Scale SST Variability

In addition to the late Holocene (1,100–600 cal yr BP) cooling transition, the filtered MD07-3093 record highlights SST variability on multicentennial timescales over the last 1,200 cal yr BP. This includes multicentennial warm periods from 1,200 to 950 and 500 to 200 cal yr BP and cool periods from 950 to 500 cal yr BP and 200 cal yr BP to present (Figure 6a). The mean (95%) uncertainty on the age of the SST record (±90 yr) is smaller than the period of this multicentennial variability. Multicentennial variability is evident in South American lake temperature records, records of SAM, Northern Hemisphere temperature records, and records of ENSO. Below, we discuss the possible mechanistic links to southern Chilean margin SST.

In terms of South American lake temperature records, Laguna Escondida (45°31′S, 71°49′W) exhibits some similarities to our SST record (Figure 6b), with relatively warm conditions from 1,050 to 750 BP, 1 °C cooler conditions from 750 to 500 cal yr BP, and warmer conditions from 500 to 250 cal yr BP (Elbert et al., 2013).

However, the two records differ prior to 1,050 cal yr BP. Two terrestrial temperature records from further north display quite different multicentennial-scale variability to our record: Laguna Aculeo (33°50′S; 70°54′W) displays warm conditions from 850–650 cal yr BP and 1 °C cooler conditions from 650–250 cal yr BP (Figure 6c), almost in antiphase to Laguna Escondida and MD07-3093. Laguna Chepical (32°16′S; 70°30′W) displays a slightly warmer phase 950 to 500 cal yr BP and two 0.5 °C cooler phases between 500 and 100 yr BP (de Jong et al., 2013; Figure 6d). The pollen record from Lago Cipreses located further south (51°17′S; 72°50′W) displays a different evolution (Figure 6e) and was interpreted in terms of SAM: Cold and wet conditions during the periods 800–100 and 1,400–1,100 cal yr BP were interpreted as negative SAM, while warm and dry conditions during the period 1,100–800 cal yr BP and over the last 100 yr were interpreted as positive SAM (Moreno et al., 2014). The discrepancies between the lake records and MD07-3093 SST may reflect regional climate variability (Villalba et al., 2003), and it would be expected that this would be more effectively captured in the smaller lake catchments than in a marine record.

Other records have also been interpreted in terms of SAM variability. Increased dust in the WAIS Divide ice core between 900 and 550 cal yr BP, broadly coeval with the MCA (1,000 to 700 cal yr BP), was interpreted as positive SAM (Koffman et al., 2013). Changes in the SHW have been shown to be sensitive to solar variability, and climate modeling suggests a poleward shift of the SHW during the MCA (Varma et al., 2011). Ice cores provide mixed evidence for multicentennial timescale SAM variability. There is evidence from the DSS (Law Dome) ice core for multicentennial temperature variability (Figure 7b): Cooler conditions during the MCA and warmer conditions during the LIA would support positive SAM during the MCA and negative SAM during the LIA. At this site, however, the influence of ENSO must be borne in mind (Vance et al., 2013). In contrast to DSS (Law Dome), however, there is no evidence for a warm MCA and cool LIA from the JRI ice core (Figure 5j), as would be expected from positive and negative SAM phases, respectively. Thus, the expression of SAM is rather inconsistent throughout South America and Antarctica. Chilean margin SSTs from MD07-3093 display relatively cool conditions between 950 and 500 cal yr BP (Figure 7a). Based on instrumental data (Figure 1c), this would point to negative SAM, rather than positive SAM, in disagreement with most of the records described above. Moreover, we note the relatively small effect of SAM on Chilean margin SST on instrumental timescales. Consequently, it seems unlikely that multicentennial SAM variability alone was the main driver of Chilean margin multicentennial SST.

Chilean margin multicentennial SST variability appears to display an almost antiphase relationship to temperature in the Northern Hemisphere (Figure 7c). The periods of cool conditions (950 to 500 cal yr BP and 200 cal yr BP to present) in our record are broadly coeval with the warm conditions in the Northern Hemisphere (MCA; 1,000 to 700 cal yr BP and the twentieth Century warming), while the period of warm conditions in our record (500 to 200 cal yr BP) is broadly coeval with cool conditions in the Northern Hemisphere (LIA; 550 to 100 cal yr BP). The two regions may be mechanistically linked via AMOC and the internally driven multicentennial timescale variability of the Southern Ocean deep convection (SOCV; Martin et al., 2013). The multicentennial variability is driven by processes internal to the Southern Ocean (buildup of heat at intermediate depth or freshwater at the surface), which have been shown to oscillate on timescales of a few centuries and result in surface temperature changes in the Southern Ocean and southern Chile margin (Latif et al., 2013; Martin et al., 2013; Zhang, Delworth, & Jia, 2017). Reduced (increased) AABW formation is also associated with increased (reduced) North Atlantic Deep Water formation and strengthening (weakening) of AMOC, via the bipolar seesaw (Martin et al., 2013, 2015). This would result in warming (cooling) in the North Atlantic region at a similar timing to the cooling (warming) in the Southern Ocean and Chilean margin and could therefore explain the antiphase behavior with the Northern Hemisphere (Figures 7a and 7c). It is also possible that the AMOC changes and Southern Ocean cooling acted as a coupled feedback (Zhang, Delworth, & Zeng, 2017).

ENSO records display clear variability on multicentennial timescales (Yan et al., 2011), and this would be an alternative mechanism to explain the multicentennial Chilean SST variability. Instrumental data show that El-Niño leads to warm southern Chilean margin SSTs and La-Niña tends to cool SSTs (Figures 1b, 2b, and 2c). Based on this, cooler Chilean margin SSTs from 950–500 cal yr BP and from 200 cal yr BP to present would point to La-Niña-like conditions, while warmer SSTs observed from 1,200–950 and 500–200 cal yr BP would suggest El-Niño-like conditions. Taken in combination with the tropical SST proxies (Cobb et al., 2003; Oppo et al., 2009) from the Central and Western Pacific, it would suggest El Niño-like conditions from 1,200 to 950 and 500 to 200 cal yr BP and La Niña-like conditions from 950 to 500 cal yr BP and from

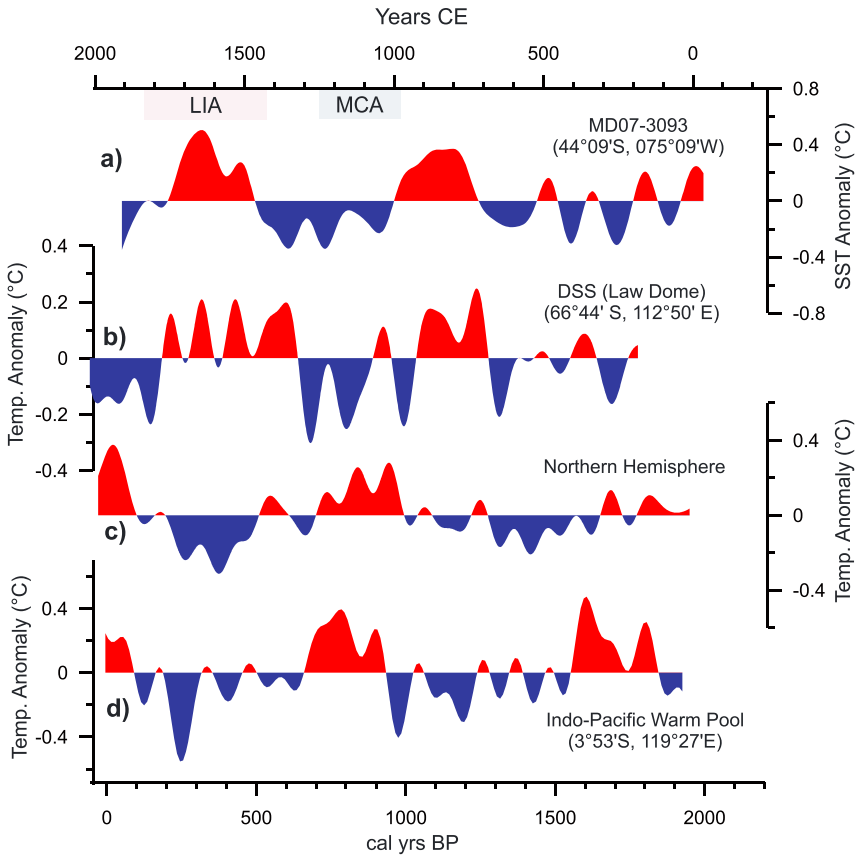

Figure 7. Multicentennial variability. (a) Southern Chile margin SST from MD07-3093. (b) DSS (Law Dome) ice core temperature anomaly (PAGES-2K-Network, 2013). (c) Northern hemisphere temperature compilation (Moberg et al., 2005). (d) Indo-Pacific Warm Pool SST record (Oppo et al., 2009), from cores BJ8 and MD60: Warmer SST reflects La-Niña like conditions. All are bandpass filtered so as to show variability with periods between 1,000 and 100 yr. SST = sea surface temperature; LIA = Little Ice Age; MCA = Medieval Climate Anomaly.

200 cal yr BP to present (Figure 7d). Nonetheless, other, often hydrological, ENSO records suggest the opposite pattern, that is, more La-Niña-like conditions during the LIA and El-Niño-like conditions during the MCA (Conroy et al., 2008; Yan et al., 2011), while other temperature records from the eastern tropical Pacific show warming since the MCA (Conroy et al., 2009). Therefore, the main cause of multicentennial variability is probably not simply related to El-Niño-like versus La-Niña-like states. Differences between the ENSO records described above may be attributable to changes in the spatial expression of ENSO anomalies over multicentennial timescales, similar to that observed over the last few decades (Sulca et al., 2018; Yeo & Kim, 2015). In a similar vein, because modern day Chilean margin SST appears to be sensitive to the phasing of individual SAM and ENSO events (see section 2.2), we propose that, as an alternative to internal SOCV, multicentennial southern Chilean margin SST variability is linked to changes in the phasing of the coupling of ENSO and SAM events. Specifically, we suggest that warmer periods (1,200–950 and 500–200 cal yr BP) could represent more frequent co-occurrence of El-Niños and positive SAM events, while cooler periods (950–500 cal yr BP and 200 cal yr BP to present) represent more frequent co-occurrences of La-Niñas and negative SAM events. Solar variability would be a potential driver of the changes in ENSO and SAM coupling. Increased (decreased) Total Solar Irradiance has been shown to promote La-Niña-like (El-Niño-like) conditions by enhancement of the trade winds (Mann et al., 2005). Similarly, the SHW are sensitive to the 11-yr solar cycle (Haigh et al., 2005) and solar variability on centennial timescales (Varma et al., 2011), and thus solar variability might be expected to exert an influence on the SAM. Therefore, it is plausible that solar variability may have controlled the phasing of ENSO and the SAM, and this remains an interesting avenue for further climate modeling research.

6. Conclusions

We have presented a high-resolution alkenone SST record from the Chile margin at 44°S spanning the last 2,300 years with decadal resolution. The record displays two main features: (1) a large magnitude cooling transition of 1.5 °C between 1,100 and 600 cal yr BP and (2) smaller magnitude multicentennial-scale variability. The cooling transition parallels other Chilean margin SST records and appears to be coeval with Antarctic cooling. We suggest that increased freshwater from sea ice in the Weddell Sea, in turn associated with stronger ENSO variability, led to a reduction of Southern Ocean deep convection. This cooled the Southern Ocean and southern Chilean margin between 1,100 and 600 cal yr BP, which resulted in a poleward shift and strengthening of the SHW, further cooling Antarctica.

Multicentennial SST variability includes a period of cooler SSTs between 950–500 cal yr BP and a period warmer SSTs 500–200 cal yr BP, broadly corresponding to the timing MCA and LIA, respectively. Thus, temperature in the SE Pacific appears to have responded out of phase with temperature in the Northern Hemisphere. The multicentennial Chile margin SST variability may reflect two potential processes. The first possibility is Southern Ocean internal variability, which oscillates unforced at multicentennial timescales. The second possibility is multicentennial variability in the phasing of individual ENSO and SAM events.

Acknowledgments
J.A.C. was funded by the Helmholtz Postdoc Programme (PD-001) and the Alfred Wegener Institute, Bremerhaven. R.D.P.-H. and R.G. were funded by CONICYT FONDAP 15110009. R.D.P.-H. also acknowledges FONDECYT 1140536 and ICM-NC120066. We would like to thank Walter Luttmer, Nilay Sasa, Nicole Syring, Ingrid Stimac, Kirsten Fahl, and Stefan Mulitza for their assistance and expertise. The data are available on the PANGAEA database (https://doi.pangaea.de/10.1594/PANGAEA.893143).

References

Abram, N. J., Mulvaney, R., Vimeux, F., Phipps, S. J., Turner, J., & England, M. H. (2014). Evolution of the Southern Annular Mode during the past millennium. *Nature Climate Change*, *4*(7), 564–569. https://doi.org/10.1038/nclimate2235

Appleby, P. G. (2001). Chronostratigraphic techniques in recent sediments. In W. M. L. J. P. Smol (Ed.), *Tracking environmental change using lake sediments. Volume 1: Basin analysis, coring, and chronological techniques* (pp. 171–203). Dordrecht, The Netherlands: Kluwer Academic Publishers.

Armour, K. C., Marshall, J., Scott, J. R., Donohoe, A., & Newsom, E. R. (2016). Southern Ocean warming delayed by circumpolar upwelling and equatorward transport. *Nature Geoscience*, *9*(7), 549–554. https://doi.org/10.1038/ngeo2731

Boës, X., & Fagel, N. (2008). Relationships between southern Chilean varved lake sediments, precipitation and ENSO for the last 600 years. *Journal of Paleolimnology*, *39*(2), 237–252. https://doi.org/10.1007/s10933-007-9119-9

Boninsegna, J. A., Argollo, J., Aravena, J., Barichivich, J., Christie, D., Ferrero, M., et al. (2009). Dendroclimatological reconstructions in South America: A review. *Palaeogeography, Palaeoclimatology, Palaeoecology*, *281*(3-4), 210–228. https://doi.org/10.1016/j.palaeo.2009.07.020

Brassell, S., Eglinton, G., Marlowe, I., Pflaumann, U., & Sarnthein, M. (1986). Molecular stratigraphy: A new tool for climatic assessment. *Nature*, *320*(6058), 129–133. https://doi.org/10.1038/320129a0

Bronk Ramsey, C. (2008). Deposition models for chronological records. *Quaternary Science Reviews*, *27*(1-2), 42–60. https://doi.org/10.1016/j.quascirev.2007.01.019

Caniupán, M., Lamy, F., Lange, C. B., Kaiser, J., Kilian, R., Arz, H. W., et al. (2014). Holocene sea-surface temperature variability in the Chilean fjord region. *Quaternary Research*, *82*(02), 342–353. https://doi.org/10.1016/j.yqres.2014.07.009

Carré, M., Jackson, D., Maldonado, A., Chase, B. M., & Sachs, J. P. (2016). Variability of ^{14}C reservoir age and air–sea flux of CO_2 in the Peru–Chile upwelling region during the past 12,000 years. *Quaternary Research*, *85*(01), 87–93. https://doi.org/10.1016/j.yqres.2015.12.002

Chaigneau, A., & Pizarro, O. (2005). Mean surface circulation and mesoscale turbulent flow characteristics in the eastern South Pacific from satellite tracked drifters. *Journal of Geophysical Research*, *110*, C05014. https://doi.org/10.1029/2004JC002628

Chaudhuri, P., & Marron, J. S. (1999). SiZer for exploration of structures in curves. *Journal of the American Statistical Association*, *94*(447), 807–823. https://doi.org/10.1080/01621459.1999.10474186

Ciasto, L. M., & Thompson, D. W. (2008). Observations of large-scale ocean-atmosphere interaction in the Southern Hemisphere. *Journal of Climate*, *21*(6), 1244–1259. https://doi.org/10.1175/2007JCLI1809.1

Cobb, K. M., Charles, C. D., Cheng, H., & Edwards, R. L. (2003). El Nino/Southern Oscillation and tropical Pacific climate during the last millennium. *Nature*, *424*(6946), 271–276. https://doi.org/10.1038/nature01779

Conroy, J. L., Overpeck, J. T., Cole, J. E., Shanahan, T. M., & Steinitz-Kannan, M. (2008). Holocene changes in eastern tropical Pacific climate inferred from a Galápagos lake sediment record. *Quaternary Science Reviews*, *27*(11-12), 1166–1180. https://doi.org/10.1016/j.quascirev.2008.02.015

Conroy, J. L., Restrepo, A., Overpeck, J. T., Steinitz-Kannan, M., Cole, J. E., Bush, M. B., & Colinvaux, P. A. (2009). Unprecedented recent warming of surface temperatures in the eastern tropical Pacific Ocean. *Nature Geoscience*, *2*(1), 46–50. https://doi.org/10.1038/ngeo390

de Jong, R., von Gunten, L., Maldonado, A., & Grosjean, M. (2013). Late Holocene summer temperatures in the central Andes reconstructed from the sediments of high-elevation Laguna Chepical, Chile (32°S). *Climate of the Past*, *9*(4), 1921–1932. https://doi.org/10.5194/cp-9-1921-2013

Denis, D., Crosta, X., Barbara, L., Massé, G., Renssen, H., Ther, O., & Giraudeau, J. (2010). Sea ice and wind variability during the Holocene in East Antarctica: Insight on middle–high latitude coupling. *Quaternary Science Reviews*, *29*(27-28), 3709–3719. https://doi.org/10.1016/j.quascirev.2010.08.007

Ding, Q., Steig, E. J., Battisti, D. S., & Wallace, J. M. (2012). Influence of the tropics on the Southern Annular Mode. *Journal of Climate*, *25*(18), 6330–6348. https://doi.org/10.1175/JCLI-D-11-00523.1

Elbert, J., Jacques-Coper, M., Van Daele, M., Urrutia, R., & Grosjean, M. (2015). A 600 years warm-season temperature record from varved sediments of Lago Plomo, Northern Patagonia, Chile (47°S). *Quaternary International*, *377*, 28–37. https://doi.org/10.1016/j.quaint.2015.01.004

Elbert, J., Wartenburger, R., von Gunten, L., Urrutia, R., Fischer, D., Fujak, M., et al. (2013). Late Holocene air temperature variability reconstructed from the sediments of Laguna Escondida, Patagonia, Chile (45°S). *Palaeogeography, Palaeoclimatology, Palaeoecology*, *369*, 482–492. https://doi.org/10.1016/j.palaeo.2012.11.013

Etourneau, J., Collins, L., Willmott, V., Kim, J.-H., Barbara, L., Leventer, A., et al. (2013). Holocene climate variations in the western Antarctic Peninsula: Evidence for sea ice extent predominantly controlled by changes in insolation and ENSO variability. *Climate of the Past*, *9*(4), 1431–1446. https://doi.org/10.5194/cp-9-1431-2013

Falvey, M., & Garreaud, R. D. (2009). Regional cooling in a warming world: Recent temperature trends in the southeast Pacific and along the west coast of subtropical South America (1979–2006). *Journal of Geophysical Research*, *114*, D04102. https://doi.org/10.1029/2008JD010519

Fegyveresi, J. M., Alley, R., Spencer, M., Fitzpatrick, J., Steig, E., White, J., et al. (2011). Late-Holocene climate evolution at the WAIS Divide site, West Antarctica: Bubble number-density estimates. *Journal of Glaciology*, *57*(204), 629–638. https://doi.org/10.3189/002214311797409677

Fogt, R. L., & Bromwich, D. H. (2006). Decadal variability of the ENSO teleconnection to the high-latitude South Pacific governed by coupling with the Southern Annular Mode*. *Journal of Climate*, *19*(6), 979–997. https://doi.org/10.1175/JCLI3671.1

Fogt, R. L., Bromwich, D. H., & Hines, K. M. (2011). Understanding the SAM influence on the South Pacific ENSO teleconnection. *Climate Dynamics*, *36*(7-8), 1555–1576. https://doi.org/10.1007/s00382-010-0905-0

Fogt, R. L., & Wovrosh, A. J. (2015). The relative influence of tropical sea surface temperatures and radiative forcing on the Amundsen Sea low. *Journal of Climate*, *28*(21), 8540–8555. https://doi.org/10.1175/JCLI-D-15-0091.1

Garreaud, R. (2018). Record-breaking climate anomalies lead to severe drought and environmental disruption in western Patagonia in 2016. *Climate Research*, *74*(3), 217–229. https://doi.org/10.3354/cr01505

Garreaud, R. D., Vuille, M., Compagnucci, R., & Marengo, J. (2009). Present-day South American climate. *Palaeogeography, Palaeoclimatology, Palaeoecology*, *281*(3-4), 180–195. https://doi.org/10.1016/j.palaeo.2007.10.032

Gillett, N., Kell, T., & Jones, P. (2006). Regional climate impacts of the Southern Annular Mode. *Geophysical Research Letters*, *33*, L23704. https://doi.org/10.1029/2006GL027721

Gong, D., & Wang, S. (1999). Definition of Antarctic oscillation index. *Geophysical Research Letters*, *26*(4), 459–462. https://doi.org/10.1029/1999GL900003

Gordon, A. L. (1978). Deep Antarctic convection west of Maud Rise. *Journal of Physical Oceanography*, *8*(4), 600–612. https://doi.org/10.1175/1520-0485(1978)008<0600:DACWOM>2.0.CO;2

Haddam, N. A., Siani, G., Michel, E., Kaiser, J., Lamy, F., Duchamp-Alphonse, S., et al. (2018). Changes in latitudinal sea surface temperature gradients along the Southern Chilean margin since the last glacial. *Quaternary Science Reviews*, *194*, 62–76. https://doi.org/10.1016/j.quascirev.2018.06.023

Haigh, J. D., Blackburn, M., & Day, R. (2005). The response of tropospheric circulation to perturbations in lower-stratospheric temperature. *Journal of Climate*, *18*(17), 3672–3685. https://doi.org/10.1175/JCLI3472.1

Hall, A., & Visbeck, M. (2002). Synchronous variability in the Southern Hemisphere atmosphere, sea ice, and ocean resulting from the Annular Mode*. *Journal of Climate*, *15*(21), 3043–3057. https://doi.org/10.1175/1520-0442(2002)015<3043:SVITSH>2.0.CO;2

Hendon, H. H., Lim, E.-P., Arblaster, J. M., & Anderson, D. L. (2014). Causes and predictability of the record wet east Australian spring 2010. *Climate Dynamics*, *42*(5-6), 1155–1174. https://doi.org/10.1007/s00382-013-1700-5

Holland, P. R., & Kwok, R. (2012). Wind-driven trends in Antarctic sea-ice drift. *Nature Geoscience*, *5*(12), 872–875. https://doi.org/10.1038/ngeo1627

Hosking, J. S., Orr, A., Marshall, G. J., Turner, J., & Phillips, T. (2013). The influence of the Amundsen–Bellingshausen Seas low on the climate of West Antarctica and its representation in coupled climate model simulations. *Journal of Climate*, *26*(17), 6633–6648. https://doi.org/10.1175/JCLI-D-12-00813.1

Huang, B., Thorne, P. W., Banzon, V. F., Boyer, T., Chepurin, G., Lawrimore, J. H., et al. (2017). Extended reconstructed sea surface temperature, version 5 (ERSSTv5): Upgrades, validations, and intercomparisons. *Journal of Climate*, *30*(20), 8179–8205. https://doi.org/10.1175/JCLI-D-16-0836.1

Ingram, B. L., & Southon, J. R. (1996). Reservoir ages in eastern Pacific coastal and estuarine waters. *Radiocarbon*, *38*(03), 573–582. https://doi.org/10.1017/S0033822200030101

Kaiser, J., Lamy, F., & Hebbeln, D. (2005). A 70-kyr sea surface temperature record off southern Chile (Ocean Drilling Program Site 1233). *Paleoceanography*, *20*, PA4009. https://doi.org/10.1029/2005PA001146

Kalnay, E., Kanamitsu, M., Kistler, R., Collins, W., Deaven, D., Gandin, L., et al. (1996). The NCEP/NCAR 40-Year Reanalysis Project. *Bulletin of the American Meteorological Society*, *77*, 437–471. https://doi.org/10.1175/1520-0477(1996)077<0437:tnyrp>2.0.co;2

Kissel, C., Leau, H. (2007). MD 159-PACHIDERME, PAcifique CHIli Dynamique des Eaux inteRMEdiaires à bord du Marion Dufresne. *Les rapports de campagnes à la mer*.

Koffman, B. G., Kreutz, K., Breton, D., Kane, E., Winski, D., Birkel, S., et al. (2013). Centennial-scale variability of the Southern Hemisphere westerly wind belt in the eastern Pacific over the past two millennia. *Climate of the Past*, *10*, 1125–1144.

Lamy, F., Rühlemann, C., Hebbeln, D., & Wefer, G. (2002). High-and low-latitude climate control on the position of the southern Peru-Chile Current during the Holocene. *Paleoceanography*, *17*(2), 1028. https://doi.org/10.1029/2001PA000727

Lara, A., & Villalba, R. (1993). A 3620-year temperature record from Fitzroya cupressoides tree rings in southern South America. *Science*, *260*(5111), 1104–1106. https://doi.org/10.1126/science.260.5111.1104

Latif, M., Martin, T., & Park, W. (2013). Southern Ocean sector centennial climate variability and recent decadal trends. *Journal of Climate*, *26*(19), 7767–7782. https://doi.org/10.1175/JCLI-D-12-00281.1

L'Heureux, M. L., & Thompson, D. W. (2006). Observed relationships between the El Niño-Southern Oscillation and the extratropical zonal-mean circulation. *Journal of Climate*, *19*(2), 276–287. https://doi.org/10.1175/JCLI3617.1

Locarnini, R. A., Mishonov, A. V., Antonov, J. I., Boyer, T. P., Garcia, H. E., Baranova, O. K., et al. (2013). In S. Levitus, & A. Mishonov (Eds.), *World Ocean Atlas 2013, Volume 1: Temperature* NOAA Atlas NESDIS (Vol. 73, p. 40).

Mann, M. E., Cane, M. A., Zebiak, S. E., & Clement, A. (2005). Volcanic and solar forcing of the tropical Pacific over the past 1000 years. *Journal of Climate*, *18*(3), 447–456. https://doi.org/10.1175/JCLI-3276.1

Marshall, G. J., Orr, A., Van Lipzig, N. P., & King, J. C. (2006). The impact of a changing Southern Hemisphere Annular Mode on Antarctic Peninsula summer temperatures. *Journal of Climate*, *19*(20), 5388–5404. https://doi.org/10.1175/JCLI3844.1

Marshall, J., & Speer, K. (2012). Closure of the meridional overturning circulation through Southern Ocean upwelling. *Nature Geoscience*, *5*(3), 171–180. https://doi.org/10.1038/ngeo1391

Martin, T., Park, W., & Latif, M. (2013). Multi-centennial variability controlled by Southern Ocean convection in the Kiel Climate Model. *Climate Dynamics*, *40*(7-8), 2005–2022. https://doi.org/10.1007/s00382-012-1586-7

Martin, T., Park, W., & Latif, M. (2015). Southern Ocean forcing of the North Atlantic at multi-centennial time scales in the Kiel Climate Model. *Deep Sea Research Part II: Topical Studies in Oceanography*, *114*, 39–48. https://doi.org/10.1016/j.dsr2.2014.01.018

Mayewski, P., Maasch, K., Dixon, D., Sneed, S., Oglesby, R., Korotkikh, E., et al. (2013). West Antarctica's sensitivity to natural and human-forced climate change over the Holocene. *Journal of Quaternary Science*, *28*(1), 40–48. https://doi.org/10.1002/jqs.2593

Merino-Campos, V., De Pol-Holz, R., Southon, J., Latorre, C., & Collado-Fabbri, S. (2018). Marine radiocarbon reservoir age along the chilean continental margin. *Radiocarbon*, 1–16.

Mezgec, K., Stenni, B., Crosta, X., Masson-Delmotte, V., Baroni, C., Braida, M., et al. (2017). Holocene sea ice variability driven by wind and polynya efficiency in the Ross Sea. *Nature Communications*, *8*(1), 1334. https://doi.org/10.1038/s41467-017-01455-x

Moberg, A., Sonechkin, D. M., Holmgren, K., Datsenko, N. M., & Karlén, W. (2005). Highly variable Northern Hemisphere temperatures reconstructed from low-and high-resolution proxy data. *Nature*, *433*(7026), 613–617. https://doi.org/10.1038/nature03265

Mohtadi, M., Romero, O. E., & Kaiser, J.r.m., Hebbeln, D. (2007). Cooling of the southern high latitudes during the Medieval Period and its effect on ENSO. *Quaternary Science Reviews*, *26*(7-8), 1055–1066. https://doi.org/10.1016/j.quascirev.2006.12.008

Moreno, P. I., Vilanova, I., Villa-Martínez, R., Garreaud, R., Rojas, M., & De Pol-Holz, R. (2014). Southern Annular Mode-like changes in southwestern Patagonia at centennial timescales over the last three millennia. *Nature Communications*, *5*(1). https://doi.org/10.1038/ncomms5375

Moy, C. M., Seltzer, G. O., Rodbell, D. T., & Anderson, D. M. (2002). Variability of El Niño/Southern Oscillation activity at millennial timescales during the Holocene epoch. *Nature*, *420*(6912), 162–165. https://doi.org/10.1038/nature01194

Müller, P. J., Kirst, G., Ruhland, G., Von Storch, I., & Rosell-Melé, A. (1998). Calibration of the alkenone paleotemperature index $U^{K'}_{37}$ based on core-tops from the eastern South Atlantic and the global ocean (60°N-60°S). *Geochimica et Cosmochimica Acta*, *62*(10), 1757–1772. https://doi.org/10.1016/S0016-7037(98)00097-0

Mulvaney, R., Abram, N. J., Hindmarsh, R. C., Arrowsmith, C., Fleet, L., Triest, J., et al. (2012). Recent Antarctic Peninsula warming relative to Holocene climate and ice-shelf history. *Nature*, *489*(7414), 141–144. https://doi.org/10.1038/nature11391

Neukom, R., & Gergis, J. (2012). Southern Hemisphere high-resolution palaeoclimate records of the last 2000 years. *The Holocene*, *22*(5), 501–524. https://doi.org/10.1177/0959683611427335

Neukom, R., Gergis, J., Karoly, D. J., Wanner, H., Curran, M., Elbert, J., et al. (2014). Inter-hemispheric temperature variability over the past millennium. *Nature Climate Change*, *4*(5), 362–367. https://doi.org/10.1038/nclimate2174

Neukom, R., Luterbacher, J., Villalba, R., Küttel, M., Frank, D., Jones, P., et al. (2011). Multiproxy summer and winter surface air temperature field reconstructions for southern South America covering the past centuries. *Climate Dynamics*, *37*(1-2), 35–51. https://doi.org/10.1007/s00382-010-0793-3

Oppo, D. W., Rosenthal, Y., & Linsley, B. K. (2009). 2,000-year-long temperature and hydrology reconstructions from the Indo-Pacific warm pool. *Nature*, *460*(7259), 1113–1116. https://doi.org/10.1038/nature08233

PAGES-2K-Network (2013). Continental-scale temperature variability during the past two millennia. *Nature Geoscience*, *6*(5), 339–346. https://doi.org/10.1038/ngeo1797

Paillard, D., Labeyrie, L., & Yiou, P. (1996). Macintosh program performs time-series analysis. *Eos Transactions American Geophysical Union*, *77*(39), 379. https://doi.org/10.1029/96EO00259

Park, W., & Latif, M. (2008). Multidecadal and multicentennial variability of the meridional overturning circulation. *Geophysical Research Letters*, *35*, L22703. https://doi.org/10.1029/2008GL035779

Parkinson, C., & Cavalieri, D. (2012). Antarctic sea ice variability and trends, 1979–2010. *The Cryosphere*, *6*(4), 871–880. https://doi.org/10.5194/tc-6-871-2012

Prahl, F. G., Mix, A. C., & Sparrow, M. A. (2006). Alkenone paleothermometry: Biological lessons from marine sediment records off western South America. *Geochimica et Cosmochimica Acta*, *70*(1), 101–117. https://doi.org/10.1016/j.gca.2005.08.023

Prahl, F. G., Muehlhausen, L. A., & Zahnle, D. L. (1988). Further evaluation of long-chain alkenones as indicators of paleoceanographic conditions. *Geochimica et Cosmochimica Acta*, *52*(9), 2303–2310. https://doi.org/10.1016/0016-7037(88)90132-9

Renssen, H., Goosse, H., Fichefet, T., Masson-Delmotte, V., & Koç, N. (2005). Holocene climate evolution in the high-latitude Southern Hemisphere simulated by a coupled atmosphere-sea ice-ocean-vegetation model. *The Holocene*, *15*(7), 951–964. https://doi.org/10.1191/0959683605hl869ra

Ruppert, D., Sheather, S. J., & Wand, M. P. (1995). An effective bandwidth selector for local least squares regression. *Journal of the American Statistical Association*, *90*(432), 1257–1270. https://doi.org/10.1080/01621459.1995.10476630

Schneider, W., Pérez-Santos, I., Ross, L., Bravo, L., Seguel, R., & Hernández, F. (2014). On the hydrography of Puyuhuapi Channel, Chilean Patagonia. *Progress in Oceanography*, *129*, 8–18. https://doi.org/10.1016/j.pocean.2014.03.007

Schulz, H.-M., Schöner, A., & Emeis, K.-C. (2000). Long-chain alkenone patterns in the Baltic Sea—An ocean-freshwater transition. *Geochimica et Cosmochimica Acta*, *64*(3), 469–477. https://doi.org/10.1016/S0016-7037(99)00332-4

Sepúlveda, J., Pantoja, S., Hughen, K. A., Bertrand, S., Figueroa, D., León, T., et al. (2009). Late Holocene sea-surface temperature and precipitation variability in northern Patagonia, Chile (Jacaf Fjord, 44 S). *Quaternary Research*, *72*(03), 400–409. https://doi.org/10.1016/j.yqres.2009.06.010

Shevenell, A., Ingalls, A., Domack, E., & Kelly, C. (2011). Holocene Southern Ocean surface temperature variability west of the Antarctic Peninsula. *Nature*, *470*(7333), 250–254. https://doi.org/10.1038/nature09751

Siani, G., Michel, E., De Pol-Holz, R., DeVries, T., Lamy, F., Carel, M., et al. (2013). Carbon isotope records reveal precise timing of enhanced Southern Ocean upwelling during the last deglaciation. *Nature Communications*, *4*(1). https://doi.org/10.1038/ncomms3758

Stammerjohn, S., Martinson, D., Smith, R., Yuan, X., & Rind, D. (2008). Trends in Antarctic annual sea ice retreat and advance and their relation to El Niño–Southern Oscillation and Southern Annular Mode variability. *Journal of Geophysical Research*, *113*, C03S90. https://doi.org/10.1029/2007JC004269

Steig, E. J., Schneider, D. P., Rutherford, S. D., Mann, M. E., Comiso, J. C., & Shindell, D. T. (2009). Warming of the Antarctic ice-sheet surface since the 1957 International Geophysical Year. *Nature*, *457*(7228), 459–462. https://doi.org/10.1038/nature07669

Strub, P. T., Mesias, J., Montecino, V., Ruttland, J., & Salinas, S. (1998). Coastal ocean circulation off western South America. In K. H. Brink, & A. R. Robinson (Ed,.), *The Sea* (pp. 273–312). New York: John Wiley.

Sulca, J., Takahashi, K., Espinoza, J. C., Vuille, M., & Lavado-Casimiro, W. (2018). Impacts of different ENSO flavors and tropical Pacific convection variability (ITCZ, SPCZ) on austral summer rainfall in South America, with a focus on Peru. *International Journal of Climatology*, *38*(1), 420–435. https://doi.org/10.1002/joc.5185

Talley, L. D. (1999). Some aspects of ocean heat transport by the shallow, intermediate and deep overturning circulations. In U. Clark, S. Webb, & D. Keigwin (Eds.), *Mechanisms of global climate change at millennial time scalesGeophysical Monograph* (Vol. 112, pp. 1–22). Washington, DC: American Geophysical Union.

Thompson, D. W., Solomon, S., Kushner, P. J., England, M. H., Grise, K. M., & Karoly, D. J. (2011). Signatures of the Antarctic ozone hole in Southern Hemisphere surface climate change. *Nature Geoscience*, *4*(11), 741–749. https://doi.org/10.1038/ngeo1296

Thompson, D. W., & Wallace, J. M. (2000). Annular modes in the extratropical circulation. Part I: Month-to-month variability*. *Journal of Climate*, *13*(5), 1000–1016. https://doi.org/10.1175/1520-0442(2000)013<1000:AMITEC>2.0.CO;2

Thompson, D. W. J., & Solomon, S. (2002). Interpretation of recent Southern Hemisphere climate change. *Science*, *296*, 895–899. https://doi.org/10.1126/science.1069270

Vance, T. R., van Ommen, T. D., Curran, M. A., Plummer, C. T., & Moy, A. D. (2013). A millennial proxy record of ENSO and eastern Australian rainfall from the Law Dome ice core, East Antarctica. *Journal of Climate*, *26*(3), 710–725. https://doi.org/10.1175/JCLI-D-12-00003.1

Varma, V., Prange, M., Lamy, F., Merkel, U., & Schulz, M. (2011). Solar-forced shifts of the Southern Hemisphere Westerlies during the Holocene. *Climate of the Past*, *7*(2), 339–347. https://doi.org/10.5194/cp-7-339-2011

Varma, V., Prange, M., Merkel, U., Kleinen, T., Lohmann, G., Pfeiffer, M., et al. (2012). Holocene evolution of the Southern Hemisphere westerly winds in transient simulations with global climate models. *Climate of the Past*, *8*(2), 391–402. https://doi.org/10.5194/cp-8-391-2012

Villalba, R., Lara, A., Boninsegna, J. A., Masiokas, M., Delgado, S., Aravena, J. C., et al. (2003). Large-scale temperature changes across the southern Andes: 20th-century variations in the context of the past 400 years. In *Climate variability and change in high elevation regions: Past, present & future* (pp. 177–232). Dordrecht, The Netherlands: Kluwer Academic Publishers.

Villalba, R., Lara, A., Masiokas, M. H., Urrutia, R., Luckman, B. H., Marshall, G. J., et al. (2012). Unusual Southern Hemisphere tree growth patterns induced by changes in the Southern Annular Mode. *Nature Geoscience*, *5*(11), 793–798. https://doi.org/10.1038/ngeo1613

von Gunten, L., Grosjean, M., Rein, B., Urrutia, R., & Appleby, P. (2009). A quantitative high-resolution summer temperature reconstruction based on sedimentary pigments from Laguna Aculeo, central Chile, back to AD 850. *The Holocene*, *19*(6), 873–881. https://doi.org/10.1177/0959683609336573

Vuille, M., Franquist, E., Garreaud, R., Casimiro, W. S. L., & Cáceres, B. (2015). Impact of the global warming hiatus on Andean temperature. *Journal of Geophysical Research: Atmospheres*, *120*, 3745–3757. https://doi.org/10.1002/2015JD023126

WAIS-Divide-Project-Members (2013). Onset of deglacial warming in West Antarctica driven by local orbital forcing. *Nature*, *500*, 440–444.

Yan, H., Sun, L., Wang, Y., Huang, W., Qiu, S., & Yang, C. (2011). A record of the Southern Oscillation Index for the past 2,000 years from precipitation proxies. *Nature Geoscience*, *4*(9), 611–614. https://doi.org/10.1038/ngeo1231

Yeo, S.-R., & Kim, K.-Y. (2015). Decadal changes in the Southern Hemisphere sea surface temperature in association with El Niño–Southern Oscillation and Southern Annular Mode. *Climate Dynamics*, *45*(11-12), 3227–3242. https://doi.org/10.1007/s00382-015-2535-z

Yuan, X. (2004). ENSO-related impacts on Antarctic sea ice: A synthesis of phenomenon and mechanisms. *Antarctic Science*, *16*(4), 415–425. https://doi.org/10.1017/S0954102004002238

Zhang, L., Delworth, T. L., & Jia, L. (2017). Diagnosis of decadal predictability of Southern Ocean sea surface temperature in the GFDL CM2. 1 model. *Journal of Climate*, *30*(16), 6309–6328. https://doi.org/10.1175/JCLI-D-16-0537.1

Zhang, L., Delworth, T. L., & Zeng, F. (2017). The impact of multidecadal Atlantic meridional overturning circulation variations on the Southern Ocean. *Climate Dynamics*, *48*(5-6), 2065–2085. https://doi.org/10.1007/s00382-016-3190-8